Arc and Weld Pool Behavior for Pulsed Current GTAW

High-frequency current pulsing can be used to control the geometry of a GTA weld pool

BY H. R. SAEDI AND W. UNKEL

ABSTRACT. An experimental study of pulsed current GTAW was conducted to determine the effects of frequency on the arc column and the weld pool. This investigation consisted of examining the process by: 1) a photo diode array, 2) stationary arc melt runs, and 3) split anode experiments.

The photo diode array measurement was shown to be an accurate and effective method to observe and measure the response of the arc channel width to changes in the input current in real time. Results indicated that for full sinusoidal pulsing at high frequencies ($f \sim 3000$ Hz) the current channel was "frozen" in time and did not change with the instantaneous current. Stationary arc melt runs confirmed that high-frequency sinusoidal pulsing resulted in deeper welds than those at average steady current levels.

Melt runs were made using sinusoidal pulsing with $<I> = 150$ A, an amplitude of 120 A, and varying frequencies. The melts made at 3000 Hz showed an increase of 20% in depth compared to melts made at the average steady current of 150 A, with no increase in top width.

These results show that high-frequency current pulsing changed the weld pool geometry by deepening the pool without changing the top width. Therefore, high-frequency current pulsing is an effective scheme for GTAW pool geometry control.

Introduction

Over the years, the cost of constructing critical welded structures has increased dramatically. The quality of the original weld determines the frequency of failure and repair costs. Closed-loop automatic welding is one way to effectively improve the quality and productivity of the welding process while reducing the overall cost. To achieve this, an improved physical understanding of the welding process is needed. In particular, it is necessary to understand the effects of manipulation of input variables, such as current pulsing, and the process output variable, *i.e.*, weld geometry.

The weld quality is often characterized by the pool geometry. Generally, a high-quality weld will have a large depth-to-width ratio and an equiaxed dendritic grain structure. Research has shown that convection is the dominant factor for the weld pool growth (Refs. 1, 2). Therefore, the ability to control convection is necessary to change the weld pool geometry and its metallurgical structure (Refs. 3, 4). The following is a list of the forces contributing to convection within the pool:

1) Electromagnetic force ($J \times B$) generated by the action of current density on the induced magnetic field.
2) Surface tension forces due to the temperature gradient.
3) Arc pressure and shearing force on the surface of the weld pool due to the plasma jet momentum.
4) Buoyancy forces due to changes in temperature of the melt.

Examination of these forces reveals that electromagnetic forces push the fluid radially inward and then down the axis, while surface tension forces can cause a fluid motion either radially inward or outward depending on the sign of the surface tension temperature coefficient (Ref. 5). The arc pressure pushes the fluid down, while its shearing force pushes the fluid outward—Fig. 1. Buoyancy forces push the fluid up and then in a radially outward direction.

An order-of-magnitude analysis (Refs. 6–8) has shown that only the buoyancy effect can be neglected and that within the range of "normal" welding conditions, the situations can be such that one of the forces can dominate the others. To illustrate this, consider a spot weld. At high enough currents ($I > 300$ A), the arc pressure force becomes large enough to cause the melt to splatter away from under the arc-scorching effect (Ref. 9). For moderate currents and not very thick plates, the electromagnetic force dominates, generally resulting in a deeper pool. On the other hand, for moderate currents and thick plates with strong impurities in the metal or on the surface, the surface tension forces dominate. If the surface tension decreases with temperature, the pool will tend to be very wide.

KEY WORDS

Plasma Arc Column
Pulsed Current GTAW
Weld Pool
Photo Diode Array
Stationary Arc Melt
Split Anode Experiment
Arc-Melt Runs
Sinusoidal Pulsing
HF Current Pulsing
Weld Pool Geometry

Ways to Control the Arc and the Weld Pool

The need for a weld pool control arises from the desire to remove variations in the bead shape, resulting from minor changes in the material composition or changes imposed by the work environment. Different process modification schemes are needed to bring about such control. These schemes need to have the welding device variables placed under control to have as direct regulation of a single output variable as possible. For example, it may be desirable to control the weld depth independently from the top width by varying the current. Most process modifications require some kind of change in the forces within the arc and the melt. The nature of these forces depends on the characteristics of the arc, such as current, temperature and the resulting heat distribution within the arc. Manipulation of the stirring forces is a

H. R. SAEDI and W. UNKEL are with the Department of Mechanical Engineering, MIT, Cambridge, Mass.

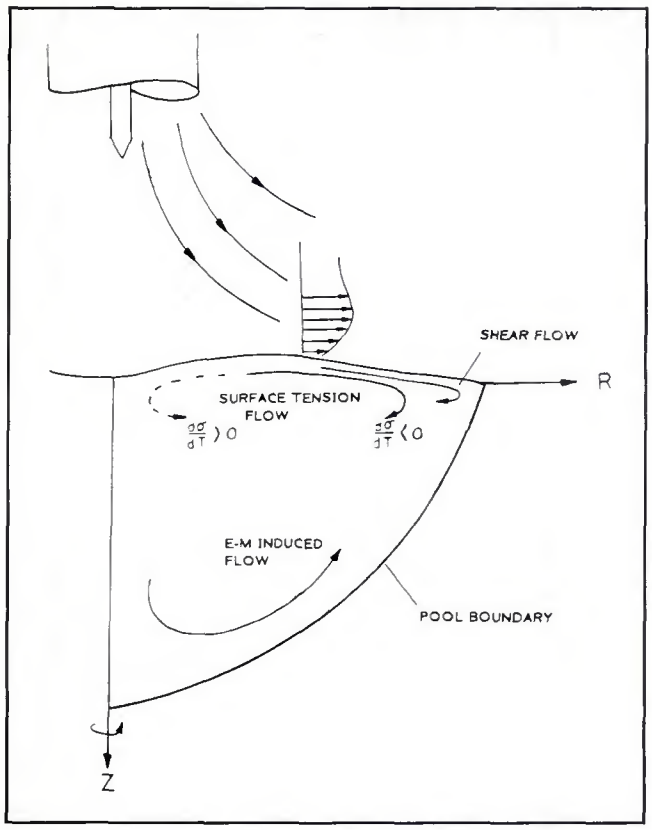

Fig. 1—Forces affecting the stirring inside the weld pool

promising scenario for the desired process modification that could be used in an active control arrangement. Two possible methods of manipulating these factors are:

1) imposing an external magnetic field, and
2) current pulsing.

If an external axial magnetic field is imposed on the arc, the internal motion of the weld pool would be circular around the axis of the electrode. This rotation would give rise to an asymmetric heat flow in the pool with respect to the welding center line, causing the weld bead to be skewed relative to the latter. In order to correct this, the applied magnetic field has to be reversed periodically (Ref. 10). This ensures a reversal in the direction of stirring. Despite this, the resulting weld pool geometry, though of homogeneous properties, will be shallow and wide. This choice of control will not be pursued during this work.

Current pulsing has a two-fold effect. First, it results in an increased plasma momentum, and secondly, it increases the value of the electromagnetic force inside the weld pool. This can be explained in the following manner. The electromagnetic body force is a result of the action of current on its induced magnetic field, *i.e.*, $F \sim J \times B$ where J is the current density and B is the magnetic field. Since both J and B are proportional to the average current, $\langle I \rangle$, the body force will be proportional to the current's squared average $\langle I^2 \rangle$ (Refs. 11, 12). Mathematically, this parameter is

$$\langle I^2 \rangle = \frac{\int_0^\tau I^2(t)\, dt}{\tau}$$

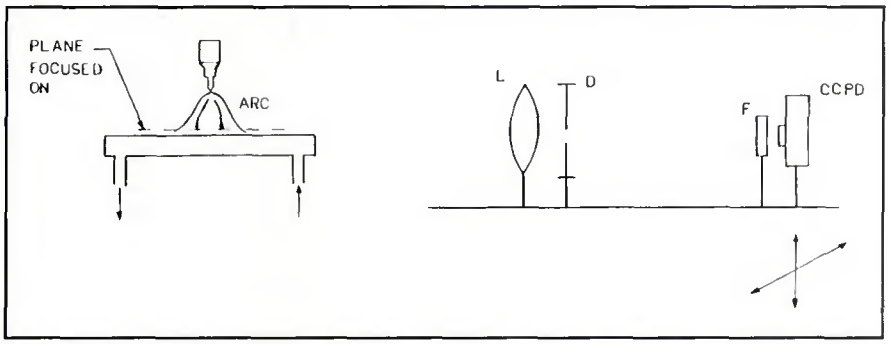

Fig. 2—Schematic of the photo diode array setup. L—Lens; D—diaphragm; F—filter

It can be shown that for any pulse shape superimposed on the average DC value, the value of $\langle I^2 \rangle$ is greater than the one for a steady value (DC) case (which is the same as $\langle I \rangle^2$). In fact,

$$\langle I^2 \rangle = n \cdot \langle I \rangle^2$$

and therefore,

$$F|_{pulsing} \sim n \cdot F|_{DC}$$

where n is a (pulse) shape factor and is 1.5 for full sinusoidal pulses ($I = I_o + I_o \sin(2\pi ft)$). From this simple order-of-magnitude argument, one can deduce that current pulsing increases the electromagnetic body force and that consequently could influence the bead geometry. Furthermore, the average heat input to the plate, $\langle I.V \rangle$, would be close to that of a constant current case, hence decoupling the arc thermal effect. This decoupling effect becomes more realistic for high-frequency pulsing since the weld pool thermal time constant is of the order of a few seconds. Earlier studies (Refs. 13, 14) have revealed some advantages of pulsed GTAW, but unfortunately the investigations were limited to a small range of welding parameters.

In this report, a systematic investigation is presented which shows the importance of current pulsing as a control scheme for the pool geometry in GTAW. The experimental work consisted of three tests. First, a photo diode array was used to investigate the arc behavior under current pulsing condition. Secondly, stationary arc tests were made to observe weld pool behavior for the pulsed current cases. Finally, a split anode setup was used to investigate the current distribution at the anode surface.

Experimental Apparatus and Procedure

To establish a fundamental understanding of the effects of current pulsing on the arc/pool interaction, experiments were run for stationary arcs using steel and water-cooled-copper anodes. The emphasis of the experiments was to determine the effects of the pulse frequency on the arch channel and the geometry of the weld pool.

The Stationary Rig

A stationary rig was chosen in order to simplify the experimental configuration and the necessary analysis. A conventional three-phase power supply powered the arc. This power supply was capable of delivering 450 A at 38 V. The open circuit voltage could be adjusted with a variable transformer booster included in the power supply. The maximum open circuit voltage was 55 V.

To control the current delivered to the arc, the output of the power supply was

connected to the transistorized current regulator (Ref. 15). With this regulator, the arc current could be varied, in any shape up to 3000 Hz, from 0 to 300 A, by using a function generator supplying 0 to 10 V.

Throughout the entire experimental program, the cathode was a 2.38-mm (3/32-in.) diameter, 2% thoriated tungsten electrode. The tungsten rods were approximately 76 mm (3 in.) long and had a finely ground tip with a solid angle of 30 deg ± 0.5 deg. A 9.5-mm (3/8-in.) diameter alumina nozzle was used and the electrode was positioned to clear the nozzle by 6.35 mm (1/4 in.). Pure argon, at 28 cfh (59 L/min), was the shielding gas throughout the study.

An electrical shunt was used to measure the current delivered to the cathode. These signals were amplified by using a differential input amplifier.

All of the experiments used either a direct water-cooled anode or one with a surrounding water-cooled jacket. Therefore, the total heat delivered to the anode was determined by calculating:

$$Q = \dot{m}\, c\, \Delta T$$

where m is the mass flow rate of the water flowing in the channels, and ΔT is the water temperature rise between the inlet and outlet of the channels. To ensure a smooth flow rate, the main water inlet to the apparatus was connected to a pressure regulator. The cooling water flow rate was measured by readings from a differential pressure transducer. Readings from the pressure drop across the inlet/outlet of anode cooling passages were converted to mass flow rate by using a calibration chart. This chart was produced based on calibration experiments on the actual apparatus.

Iron-constantan thermocouples in the inlet and outlet were used to determine temperature rise of water flowing through the cooling passages. Readings from the thermocouples were amplified 100× using a differential input amplifier.

A linear voltage displacement transducer (LVDT) was used to give an accurate position of the arc. These readings were primarily needed for the split anode experiments. The torch was connected to a traverse mechanism capable of moving the arc position in vertical and horizontal planes.

All of the electrical signals from the instruments described above were recorded on a computer. The data acquisition software system used was UnkelScope (© 1984 MIT), which allowed for online data manipulation.

Charge Coupled Photo Diode Array and Test Arrangement

Radiation intensity of the plasma arc was measured by use of a charge coupled photo diode (CCPD) array, manufactured by EG&G. The CCPD array used was sensitive to light (over a wide wavelength range of 4000–12,000 Å) and produced a voltage signal varying in strength based on the intensity and duration of the emitted light upon the diode elements. The photo diode array consisted of 256 elements and the charge stored by them was transformed to a storage register and then read sequentially by a sample and hold circuit. The output of the CCPD was displayed on an oscilloscope, of which pictures of the trace could be taken.

The light falling on the diode elements was focused and controlled by a lens and a diaphragm mounted on an optical rail. A combination of a green and/or neutral density filter was used to prevent the diodes from saturating in the high-intensity light. The entire setup was enclosed within a black box to minimize surrounding radiation interference. Figure 2 shows a schematic diagram of this setup.

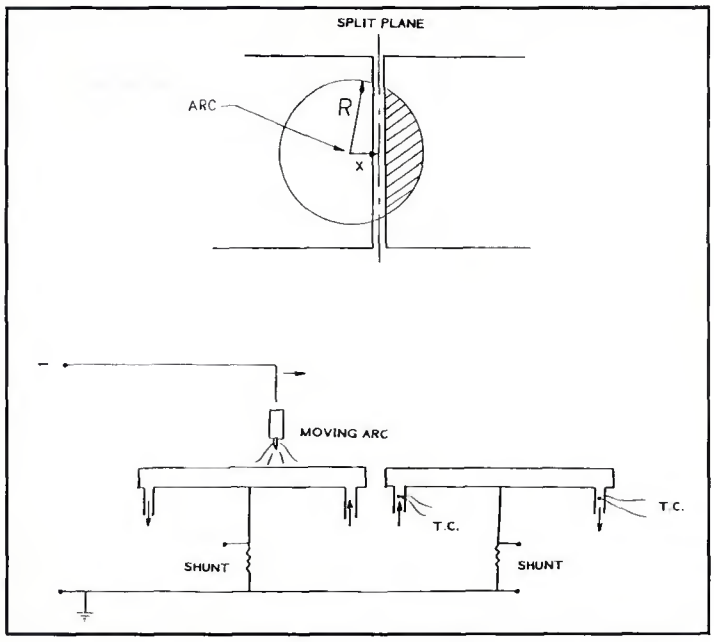

Fig. 3 — Split anode arrangement

Test Procedure

Since a qualitative pictorial review was not sufficient in this study, the photo diode array had to be calibrated to give meaningful results. It should be noted that the 256 diode elements were spread across 4 mm (0.16 in.). Therefore, the objective of calibrating the photo diode

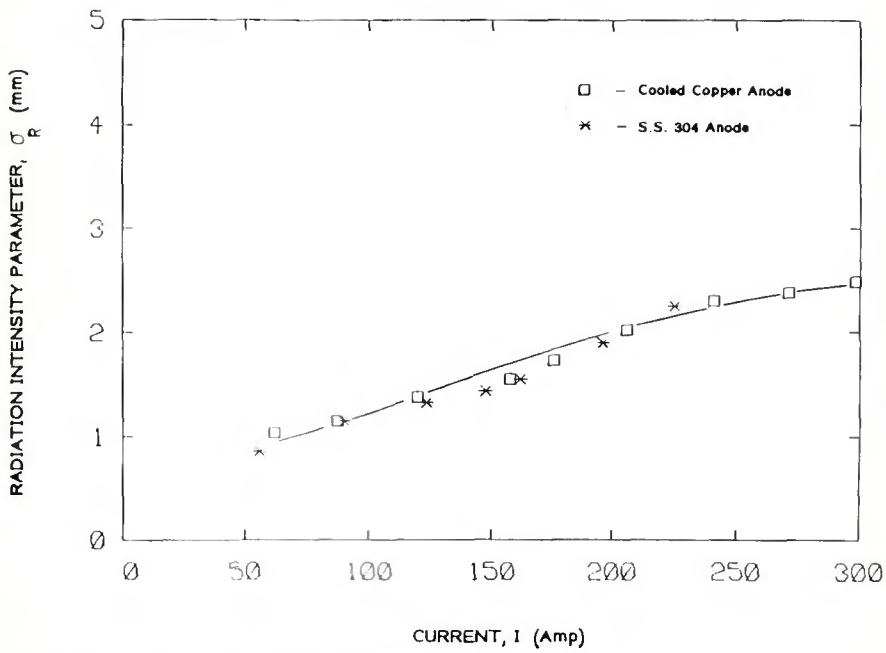

Fig. 4 — Radiation intensity distribution parameter for 4-mm arc

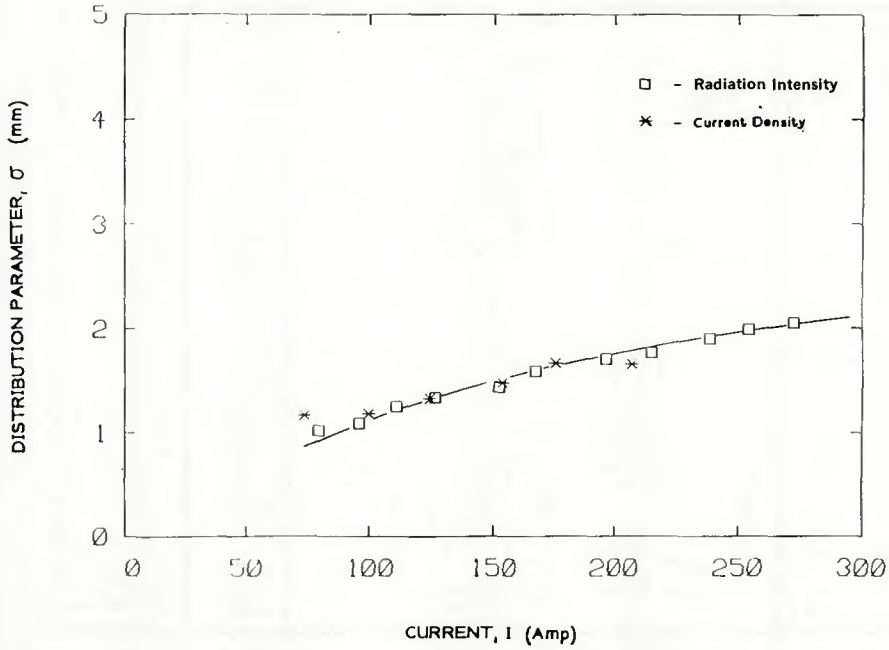

Fig. 5—Comparison between radiation intensity and current density distribution parameters for 2-mm arc

array was to find the correlation between the size of the object emitting the light and that falling on the diodes. This was accomplished by shining a laser beam behind an object of known dimensions; this produced a dark region on the photo diode array. Measurements of the length of this region made from the scope trace yielded the conversion from the image size to the object size.

At the beginning of each run, an arc was established far away from the plane in focus with the optical arrangement. The arc was moved slowly toward this plane and allowed to stabilize. This ensured an axisymmetric arc. If the scope trace or visual examination showed any asymmetry due to arc blow, the test was terminated. Through all the experiments, the photo diode array was focused on a plane 0.01 mm above the anode surface.

These experiments were performed for a variety of current levels and pulse frequencies: $10 < f < 3000$ Hz. The electrode was set at different heights above the anode surface. For each case, pictures of the photo diode trace were taken.

The above procedure and experiments were done using both water-cooled copper, and stainless steel anodes. In the former case, no melting was allowed at the anode, but in the latter, a weld pool was formed, and therefore, there was an interaction between the plasma arc and the weld pool.

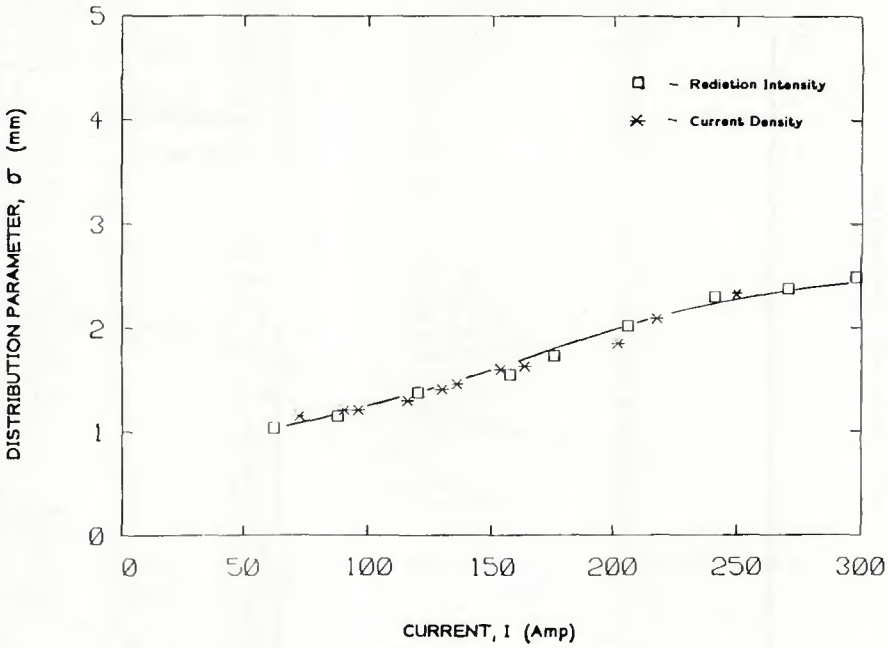

Fig. 6—Comparison between radiation intensity and current density distribution parameters for 4-mm arc

Weld Pool Tests

A series of tests was needed to establish the effect of current pulsing on the weld pool geometry. Since an objective of this work was to establish current pulsing as a possible means of controlling the weld pool geometry, experiments were run to reveal the weld pool geometry response to a pulsing scheme. Finally, other important factors, such as the arc length, used in conjunction with pulsing were to be tested. In this manner, a set of data was obtained for different transients, which revealed important features, such as typical time constants and rise time for the pool depth change.

Apparatus

In a real welding situation, a weld pool is formed along the seam of the two plates that are to be joined. In this experimental study, simplifications were made to ensure an axisymmetric weld pool. This was achieved by melting a single plate cooled equally around its circumference. This type of arrangement yields a consistent weld every time in terms of the geometry of the weld pool and its metallurgical structure.

The anode consists of a 304 stainless steel plug, 22.22 mm (⅞ in.) in diameter and 7.62 mm (0.3 in.) thick, silver soldered to the copper block. The copper block had internal cooling channels around the hole that housed the stainless steel plug. This feature ensured a nearly uniform cooling of the plug.

Procedure

At the beginning of each experiment, the electrode was set at a known height above the center of the plug. An arc was struck for a preset value of current, amplitude and frequency. Due to limitations of the current controller, the maximum sinusoidal current pulse obtained was between 30 and 270 A, in the range of $0 < f < 3000$ Hz.

For each test, a weld pool was made and allowed to reach steady state. At this point, the arc was turned off and the steel plug was removed from the copper housing and a cut was made through the center of the weld, so that one of the halves would contain the centerline plane

of the melt. To obtain the information about the weld pool geometry and the heat-affected zone, these cut specimens were mounted, polished and etched.

Two etching techniques were used: mechanically rubbing Kallings reagent on the surface, or electro-etch using 2% nital solution. Both methods yielded satisfactory results. At this point, a macro-picture of the melt was taken, and width and depth of penetration were measured.

The Split Anode Experiments

Apparatus

A split anode arrangement was used to find the current density distributions. This kind of arrangement had been used before by several investigators (Refs. 16–20) to determine the distribution parameters for the steady current case.

The apparatus consisted of two oxygen-free, high-conductivity (OFHC) copper blocks with internal cooling channels, as shown in Fig. 3, separated by 0.075 mm. Water was used as the coolant fluid to prevent any melting of the anode and as a means of measuring the heat input to each of the copper blocks. For each block, water impinged near the split interface and would flow away and exit from the far side of the block—Fig. 3. In this manner, the water stream would carry as much heat as possible away from the arc region, preventing local melting of the copper anode.

Experimental Procedure

Since the position and arrangement of the two copper blocks were crucial in these tests, every effort was made to ensure that the blocks were completely level with each other and there was a uniform spacing between them. Having set the current level and the arc length using the vertical traverse at a given value, an arc was established by striking a copper contact between the cathode and the copper plates far from the split interface. After the arc had stabilized, the arc was moved slowly toward the interface. During this time, measurements of current, voltage, diplacement, water temperature rise, and water flow rate were recorded using the computerized data acquisition system.

Experimental Results

In this section, the results of the experiments will be presented. The first part deals with the photo diode array experiments and discusses the nature of arc intensity and its relation to the arc (current) channel, and the behavior of the arc under current pulsing. Later, the response of the weld pool under current pulsing is discussed. Finally, some general results from the split anode experiments are given. These results were used in conjunction with the result of the first part of the photo diode array experiments.

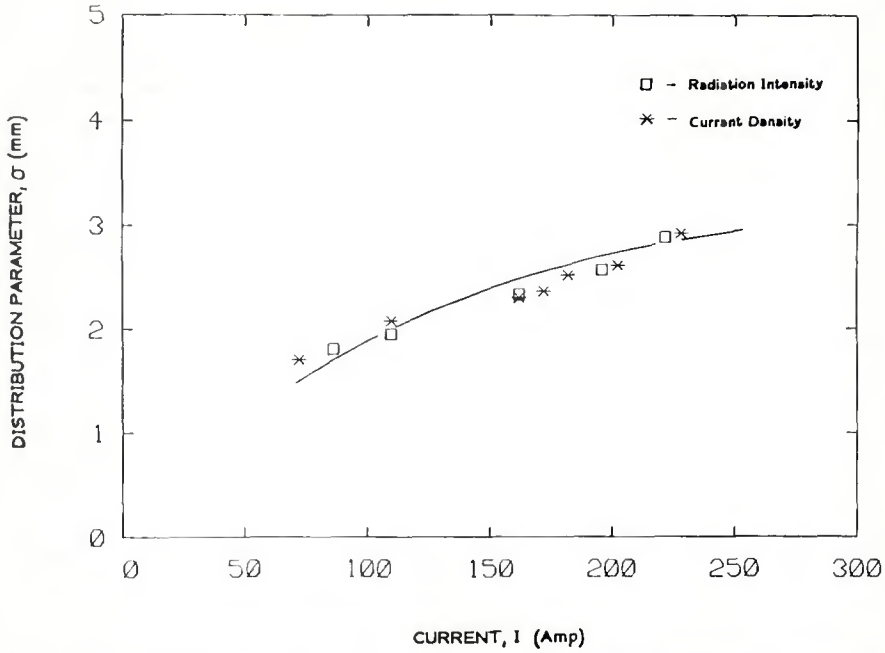

Fig. 7—Comparison between radiation intensity and current density distribution parameters for 6.3-mm arc

Photo Diode Array Experiments

Steady Current Experiments

The electric signal traces from the photo diode array showed that the plasma arc light intensity distribution can be approximated as a Gaussian type. Gaussian distributions are described by a decay radius, distribution parameter σ, corresponding to the radial distance where the density function drops to 60% of its maximum value. Therefore, direct measurements from the pictures taken from the oscilloscope were used to find the light intensity distribution parameter—Fig. 8.

Measurements taken from the arc established on the water-cooled copper plate and the stainless steel anodes showed that within the measurement accuracy, the light intensity parameters were the same—Fig. 4. This result is of great interest since for different anodes, the metal vapor generated is expected to affect the mean electrical conductivity of the arc and therefore, the arc width (current channel).

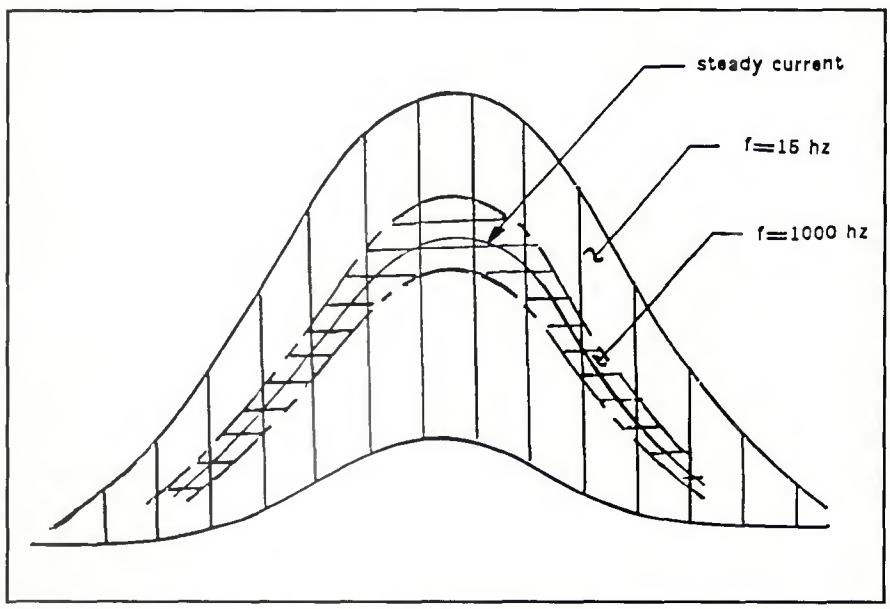

Fig. 8—Traces of photo diode array response to the arc pulsing

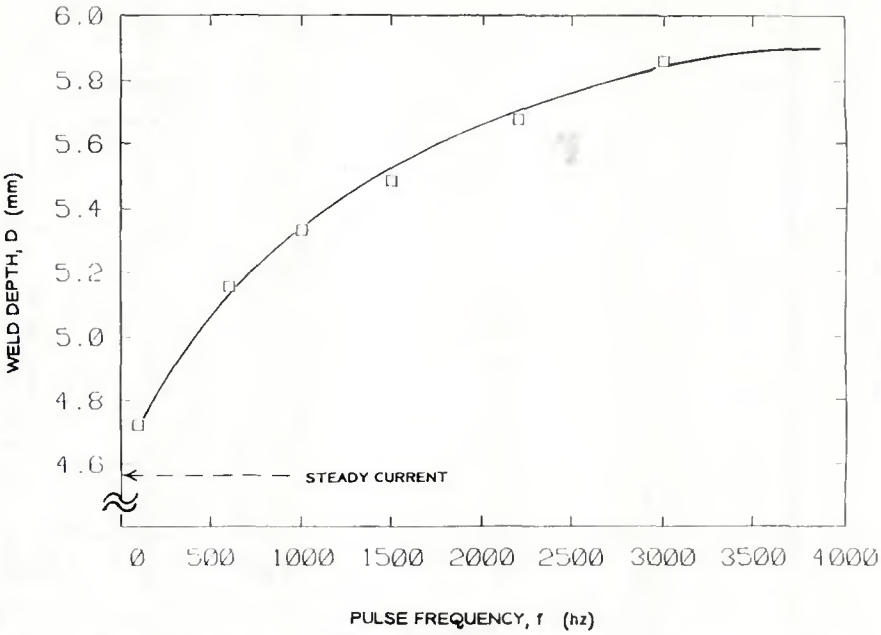

Fig. 9—Weld pool depth versus frequency for 4-mm arc pulsed sinusoidally (<I> = 150 A, amplitude of 120 A)

Comparison of the radiation and current distribution parameters obtained by split anode experiments (this is discussed in the following sections) for different arc length and current levels revealed that the radiation parameter qualitatively followed that of the current parameter. These comparisons are shown in Figs. 5-7. Therefore, when a knowledge of the current distribution is needed, photo diode trace measurements, which are very fast and easy, could be substituted for the very cumbersome split anode experiments. These findings imply that the photo diode arrays can be used as sensors to estimate the current density distribution. This would be of importance for a control process since a knowledge of the current distribution is needed for calculation of the electromagnetic body force in the weld pool.

Current Pulsing Experiments

The second set of experiments was aimed at the arc radiation intensity response to the current pulsing. The findings of these experiments proved to be very important in establishing the role of the current pulsing as a control scheme for GTAW. As expected, when (sinusoidal) current pulsing was applied, the radiation intensity trace fluctuated between two extremes corresponding to the variations in the arc column, as shown in Fig. 8. A careful analysis of these traces showed that for a low-frequency pulse, $I: I_{min} < I < I_{max}$, the upper and lower traces of the fluctuation correspond to the traces for the DC currents of I_{min} and I_{max}, respectively. This behavior held true for frequencies up to approximately 500 Hz. Beyond this frequency, the amplitude of the observed fluctuation diminished. As the frequency was increased from 500 Hz to 3000 Hz, the amplitude of the fluctuation dropped to zero, and in effect (for the entire pulse cycle), the radiation trace matched that of the DC current at the average value of the pulse.

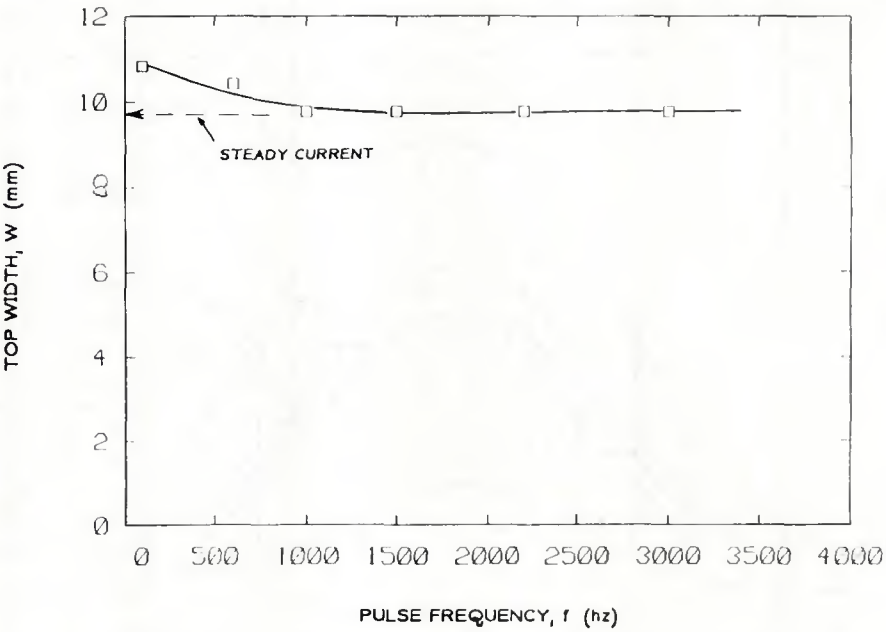

Fig. 10—Top width of weld versus frequency for 4-mm arc pulsed sinusoidally (<I> = 150 A, amplitude of 120 A)

Discussion

Experiments using the split anode arrangement had shown that the arc is in a quasi-equilibrium for pulsed current at 200 Hz and slower (Ref. 12). This conclusion was based on the observation that the current distribution for the minimum and maximum peak of the pulse matched the distributions corresponding to the steady current case at these values. These results were in agreement with the findings of the photo diode array measurements for low-frequency current pulsing (f < 500 Hz), *i.e.*, the effective current channel changed with the instantaneous current.

The results for high-frequency pulsing (f ~ 3000 Hz) indicated that the current distribution would remain constant at a value corresponding to the average value of pulsed current over the frequency cycle. In other words, for high frequencies, the arc appears to be frozen in time. This behavior at high-frequency pulsing was shown to dramatically increase the electromagnetic force generated in the weld pool compared to that of the current level at the average value of the pulse (Ref. 12). Indeed, by solving the Maxwell equations, it can be shown that the electromagnetic forces for the high-frequency pulsing are higher than those for the low-frequency pulsing.

Weld Pool Experiments

Geometry of the weld pool changes with current pulsing. For each run, the depth and top width of the weld pool were measured from the macro-pictures of the pool cross-sections. Plots of width, depth and depth/width versus frequency were made. Figures 9-11 show these plots for the case where the current was sinusoidally pulsed between values of 30 and 270 A, <I> = 150 A. The results clearly show that the weld pool deepens

when the current is pulsed (f > 100 Hz). The increase in the weld pool becomes more noticeable for frequencies above 500 Hz. The weld pool depth versus frequency plot (Fig. 9) suggests that the depth reaches the limit of a plateau for the frequency of 3000 Hz. Therefore, pulsing the current at frequencies in the order of 3000 Hz would result in a deeper weld with higher depth and width, than for the one at the (average) steady current level. Since the dominating stirring force and, therefore, the main factor in shaping the weld pool for the stationary arc experiments were due to the electromagnetic forces (Ref. 12), it can be deduced that high-frequency current pulsing increases the electromagnetic stirring within the melt. This is in agreement with the results established by the photo diode array measurements. Furthermore, this result is in agreement with that found by Yamaoto, *et al.* (Ref. 12). Their work showed that the arc pressure (also electromagnetic in nature and proportional to $\langle I^2 \rangle$) increased with the pulse frequency and, for their pulse shape, the pressure reached a plateau at about 6000 Hz.

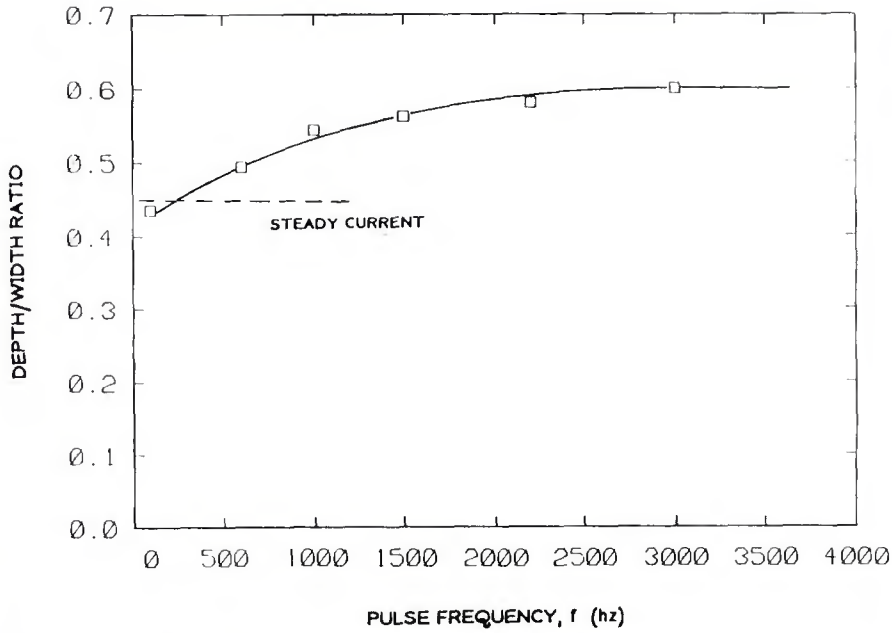

Fig. 11—Depth/width ratio versus frequency for 4-mm arc pulsed sinusoidally (<I> = 150 A, amplitude of 120 A)

Split Anode Experiments

Data Reduction

One way of finding the radial distribution of a density function, *e.g.*, current density, is to move the center of the distribution over a plane divided in half. The measurements of the total value of the function delivered to each of the halves, *i.e.*, density function × area, can be used to calculate the density function. Suppose that measurements of the total function F(x), *e.g.*, current or heat, are taken along the traversed path. Mathematically, one of these measurements is equivalent to the integration of the density function, f(r), for the shaded area in Fig. 13:

$$F(x) = 2 \int_x^R f(r)\, r \cos^{-1}(x/r)\, dr \quad (1)$$

where x is the distance from the axis of the arc to the split interface, r is the radial axis, and R is the resembling outer edge of the density function.

This equation can be rewritten to give a solution for the density function, *i.e.*, flux as a function of radius. This is done by differentiating the above, which results into an Abel integral equation with a classical solution of

$$f(r) = \frac{1}{\pi} \int_0^R F''(x)\, r \cos^{-1}(x/r)\, dr \quad (2)$$

where F″(x) is the second derivative of the measured total function.

From the above argument, it is evident that if the anode is split in two so that the two halves are thermally and electrically insulated from each other, then by traversing the arc from one half to the other, one can measure the current and heat delivered to each anode, *i.e.*, one measures the function F(x). Now, the only step to finding the sought density function distribution is a mere integration defined by Equation 2. A typical measurement for the current delivered to one of the anodes is shown in Fig. 12.

Examination of the data revealed close agreement between F(x) and an error function. To be more explicit, if F(x) can be described as

$$F(x) = A\ \mathrm{erfc}(Bx) \quad (5)$$

then evaluation of the integral in Equation 2 would yield the following for the densi-

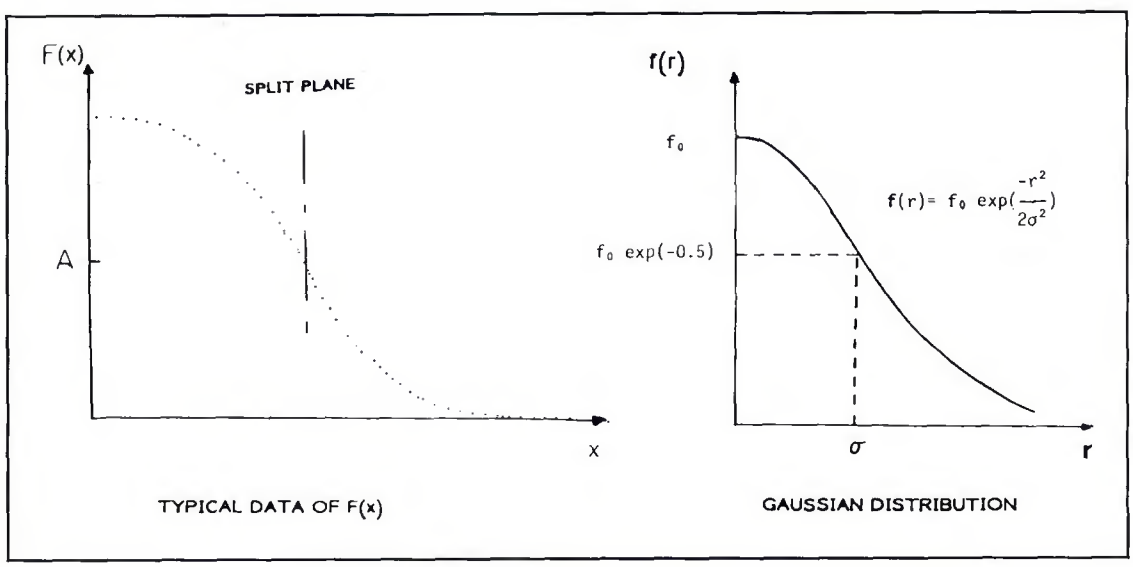

Fig. 12—Typical distributions for functions F(x) and f(r)

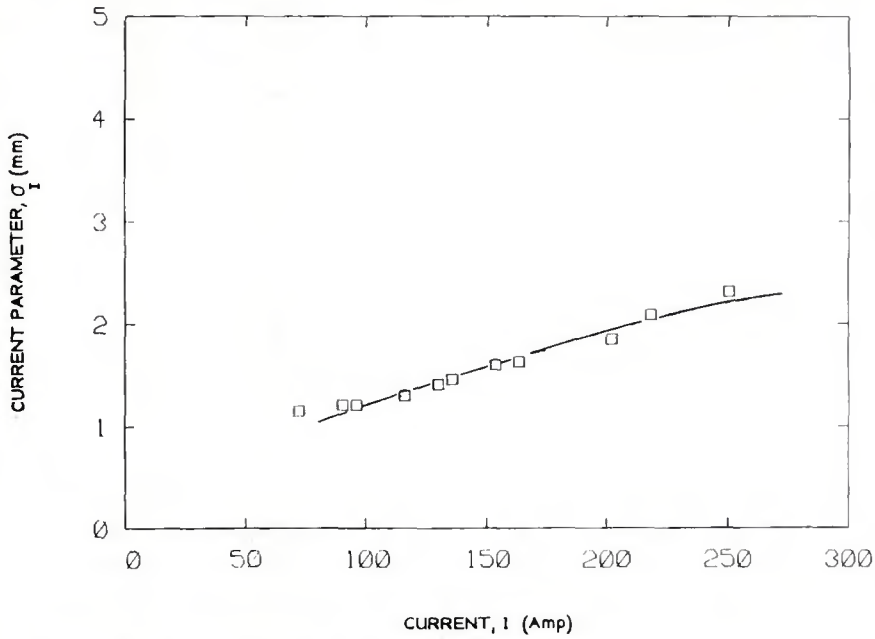

Fig. 13 — Current density parameter versus current for 4-mm arc

ty function f(r):

$$f(r) = \frac{2A}{\pi B} \exp(-B^2r^2) \qquad (6)$$

A typical curve describing the above equation is given in Fig. 12. Notice that this exponential function is a Gaussian distribution. In terms of a Gaussian distribution parameterization, one can rewrite Equation 6 in the following manner:

$$f(r) = \sigma^2 f_o \exp(-r^2/2\sigma^2) \qquad (7)$$

σ is Gaussian distribution parameter and f_o is maximum value of the density function given by Fig. 12:

$$f_o = \frac{A}{\sigma^2\pi}$$

To summarize, the above argument showed that if data taken by the split anode technique were to be curve-fitted into the error function given by Equation 5, then the density distribution function, f(r), is of Gaussian-type characterized by the curve-fit parameter, σ, and the magnitude of the peak.

A computer program was then written to process and to curve-fit the current and heat data taken by the split anode experiments.

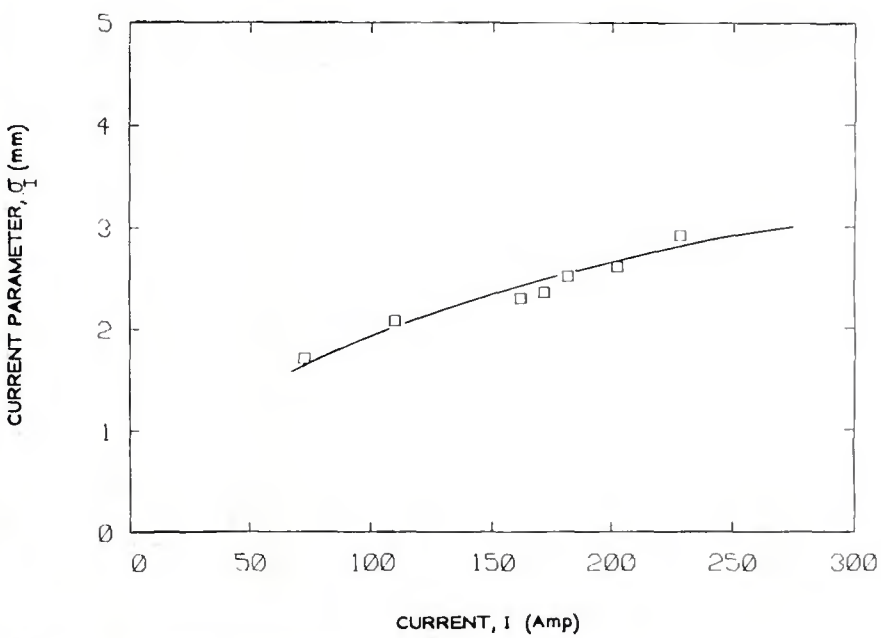

Fig. 14 — Current density parameter versus current for 6.3-mm arc

Results

The data obtained from the split anode experiments were curve-fitted according to the format described above. For each set of experiments, the distribution parameters, σ, were plotted versus the corresponding current level.

Figures 13 and 14 show the current distribution parameter versus current for arc lengths of 4 and 6.3 mm (5/32 and 1/4 in.). The results obtained from different arc lengths show that the distribution parameters increased for an increase in the arc length and current level.

Summary and Conclusions

Closed-loop control of the welding process represents a promising cost-effective approach to improving weld quality and therefore reducing total cost of producing welded structures. A multivariable control system must have as many input variables as attributes to be controlled. The possibility of using current pulsing to control arc weld pool interaction and weld size was explored.

Using a photo diode array, the light intensity and distribution from the arc was investigated. The radiation distribution parameter was found to qualitatively follow the current distribution parameter, as measured using a split anode setup. When sinusoidal shape current pulsing was applied, the output from the photo diode array showed that at low frequencies, $f < 500$ Hz, the effective current channel (the main part of the arc) changed with the instantaneous current. For high frequencies, $f \sim 3000$ Hz, the current channel was found to be "frozen" at a value corresponding to a steady arc operating at the average current. In effect, for the high-frequency pulsing, $\langle I^2 \rangle$ would be higher than for a steady arc operating at the average current value. This in turn means more vigorous electromagnetic stirring in the weld pool and therefore, deeper welds. This effect was experimentally verified by comparing melt test runs between pure DC current, I_o, and full sinusoidal pulse ($I = I_o + I_o \cdot \sin(2\pi ft)$). These experiments showed that for the high-frequency current pulsing, the weld depth increased, while the top width showed no significant change. More specifically, when current was pulsed sinusoidally between 30 and 270 A, weld depth was increased by 20% over the weld made at the average steady current level of 150 A.

The results imply that high-frequency current pulsing increases the electromagnetic stirring force in the weld pool and therefore, increases the weld depth independent of top width, resulting in a different pool shape. Thus, current pulsing can be used to control the weld pool geometry in GTAW.

References

1. Woods, R. A., and Milner, D. R. 1971. Motion in the weld pool in arc welding. *Welding Journal* 50(5):163-s to 173-s.
2. Ishizaki, K. *et al.* 1966. Penetration in arc welding and convection in molten metal. IIW 212-77-66.
3. Davies, G. J. *et al.* 1975. Solidification structure and properties of fusion welds. *Int. Metallurgical Reviews* 20:83-106.
4. Matsuda, F. *et al.* 1979. Effects of electromagnetic stirring on the weld solidification structure of aluminum alloys. Paper No. 10, *Arc Physics and Weld Pool Behavior Int. Conf.* London, England.
5. Bradstreet, B. J. 1968. Effect of surface tension and metal flow on weld bead formation. *Welding Journal* 47(7):314-s to 322-s.
6. Karniadakis, G. 1984. Development and experimental validation of a predictive model for a GTA weld pool geometry. MIT, SM thesis.
7. Oreper, G. M., and Szekely, J. 1984. Heat and fluid flow phenomena in weld pools. *J. Fluid Mechanics* 147:53-79.
8. Oreper, G. M. *et al.* 1983. Convection in arc weld pools. *Welding Journal* 62(11):307-s to 312-s.
9. Halmoy, E. 1979. The pressure of the arc acting on the weld pool. *Int. Conf. on Arc Physics and Weld Pool Behavior.* London, England.
10. Willgoss, R. A. 1981. A practical future for E.M. stirring of the weld pool. *Welding and Metal Fabrication* (5):189-197.
11. Wells, A. A. 1962. A momentum principle for arc welding. *British Welding Journal* (4).
12. Saedi, H. R. 1986. Transient response of plasma arc and weld pool geometry for GTAW processes. Sc.D. thesis, MIT.
13. Leitner, R. E. *et al.* 1973. An investigation of pulsed GTA welding variables. *Welding Journal* 52(9):405-s to 410-s.
14. Omar, A. A., and Lundin, C. D. 1979. Pulsed plasma-pulsed GTA arc: a study of process variables. *Welding Journal* 58(4):97-s to 105-s.
15. Converti, J. 1981. Plasma jets in welding. Ph.D. Thesis, MIT.
16. Nestor, O. H. Heat intensity and current density distributions at the anode of high current inert gas arcs. *Journal of Applied Physics* 33(5):1638-48.
17. Eberhart, R. C. The energy balance for a high current argon arc. *Journal of Heat and Mass Transfer* 9:939-949.
18. Shoeck, P. A. 1963. An investigation of the anode energy balance of high intensity arcs in argon. *Modern Developments in Heat Transfer,* pp.353-478.
19. Tsai, N. 1983. Heat distribution and weld bead geometry in arc welding. MIT Ph.D. thesis.
20. Eberhart, R. C., and Seban, R. A. The energy balance for a high current argon arc. *Int. J. Heat and Mass Transfer* 9:939-949.
21. Yamaoto, T. *et al.* 1976. Characteristics of high frequency pulsed DC TIG welding process. IIW 212-628-76.

WRC Bulletin 332
April 1988

This Bulletin contains two reports that characterize the mechanical properties of two different structural shapes of constructional steels used in the pressure vessel industry.

(1) Characteristics of Heavyweight Wide-Flange Structural Shapes
By J. M. Barsom and B. G. Reisdorf

This report presents information concerning the chemical, microstructural and mechanical (including fracture toughness) properties for heavyweight wide-flange structural shapes of A36, A572 Grade 50 and A588 Grade A steels.

(2) Data Survey on Mechanical Property Characterization of A588 Steel Plates and Weldments
By A. W. Pense

This survey report summarizes, for the most part, unpublished data on the strength toughness and weldability of A588 Grade A and Grade B steels as influenced by heat treatment and processing.

Publication of this Bulletin was sponsored by the Subcommittee on Thermal and Mechanical Effects on Materials of the Pressure Vessel Research Committee of the Welding Research Council. The price of WRC Bulletin 332 is $20.00 per copy, plus $5.00 for postage and handling. Orders should be sent with payment to the Welding Research Council, Suite 1301, 345 E. 47th St., New York, NY 10017.

WRC Bulletin 335
August 1988

A Review of Area Replacement Rules for Pipe Connections in Pressure Vessels and Piping
By E. C. Rodabaugh

Pressure vessel and piping codes have used the area replacement concept for at least 50 years. This concept requires that the metal cut out by an opening be replaced by reinforcement within a prescribed zone around the opening. During the past 20 years, a substantial amount of information has accumulated which indicates that the area replacement concept, in some applications, is excessively conservative. Alternative rules are given in this report for the two extremes of their application: 1) for all reinforcing in the nozzle and 2) for all reinforcing in the vessel.

Publication of this report was sponsored by the Subcommittee on Reinforced Openings and External Loadings of the Pressure Vessel Research Committee of the Welding Research Council. The price of WRC Bulletin 335 is $24.00 per copy, plus $5.00 for postage and handling. Orders should be sent with payment to the Welding Research Council, Suite 1301, 345 E. 47th St., New York, NY 10017.